ADVANCED BIOSYSTEMS
www.adv-biosys.com

Extracellular Vesicles Induce Mesenchymal Transition and Therapeutic Resistance in Glioblastomas through NF-κB/STAT3 Signaling

*Markus W. Schweiger, Mao Li, Alberta Giovanazzi, Renata L. Fleming, Elie I. Tabet, Ichiro Nakano, Thomas Würdinger, Ennio Antonio Chiocca, Tian Tian, and Bakhos A. Tannous**

Glioblastoma (GBM) is the most common primary malignant brain tumor and despite optimal treatment, long-term survival remains uncommon. GBM can be roughly divided into three different molecular subtypes, each varying in aggressiveness and treatment resistance. Recent evidence shows plasticity between these subtypes in which the proneural (PN) glioma stem-like cells (GSCs) undergo transition into the more aggressive mesenchymal (MES) subtype, leading to therapeutic resistance. Extracellular vesicles (EVs) are membranous structures secreted by nearly every cell and are shown to play a key role in GBM progression by acting as multifunctional signaling complexes. Here, it is shown that EVs derived from MES cells educate PN cells to increase stemness, invasiveness, cell proliferation, migration potential, aggressiveness, and therapeutic resistance by inducing mesenchymal transition through nuclear factor-κB/signal transducer and activator of transcription 3 signaling. The findings could potentially help explore new treatment strategies for GBM and indicate that EVs may also play a role in mesenchymal transition of different tumor types.

1. Introduction

Gliomas account for about 80% of all malignant CNS tumors, of which glioblastoma (GBM) is the most common and malignant form.[1] Despite a multimodal treatment approach including surgery, radiation, and temozolomide (TMZ) chemotherapy, the prognosis remains dismal. The Central Brain Tumor Registry reports that the five-year survival rate of adult patients with GBM is 4.3%. Although tumors may initially respond to this treatment armamentarium, recurrence remains inevitable.[2–5] Large-scale genomic, epigenomic, and transcriptomic characterization of different subtypes has provided valuable insights into the heterogeneous landscape of GBM.[6–9] Notably, comprehensive longitudinal

M. W. Schweiger, M. Li, A. Giovanazzi, Dr. R. L. Fleming, E. I. Tabet, Dr. T. Tian, Prof. B. A. Tannous
Experimental Therapeutics and Molecular Imaging Laboratory
Department of Neurology
Neuro-Oncology Division, Massachusetts General Hospital
Boston, MA 02129, USA
E-mail: btannous@hms.harvard.edu

M. W. Schweiger, M. Li, A. Giovanazzi, Dr. R. L. Fleming, E. I. Tabet, Dr. T. Tian, Prof. B. A. Tannous
Neuroscience Program
Harvard Medical School
Boston, MA 02129, USA

M. W. Schweiger, A. Giovanazzi, Prof. T. Würdinger
Department of Neurosurgery
Cancer Center Amsterdam
Brain Tumor Center Amsterdam
Amsterdam UMC
Vrije Universiteit
Amsterdam 1081 HV, The Netherlands

The ORCID identification number(s) for the author(s) of this article can be found under https://doi.org/10.1002/adbi.201900312.

DOI: 10.1002/adbi.201900312

M. Li
Department of Neurosurgery
West China Hospital
Sichuan University
Chengdu, Sichuan 610041, China

E. I. Tabet
Department of Biomedical Engineering
University of South Dakota
4800 N. Career Ave, Suite 221, Sioux Falls, SD 57107, USA

Prof. I. Nakano
Department of Neurosurgery and Comprehensive Cancer Center
University of Alabama at Birmingham
Birmingham, AL 35233, USA

Prof. E. A. Chiocca
Department of Neurosurgery
Brigham and Women's Hospital
Boston, MA 02115, USA

Dr. T. Tian
Department of Neurobiology
Key Laboratory of Human Functional Genomics of Jiangsu
Nanjing Medical University
Nanjing, Jiangsu 211166, China

analyses of the tumor transcriptome have classified GBM into three distinct subtypes: proneural (PN), mesenchymal (MES), and classical.[10] In addition to the complex intertumoral heterogeneity, single-cell RNA sequencing has revealed the presence of various transcriptome subtypes within the same tumor.[11] This intricate intratumoral heterogeneity plays a major role in rendering conventional and targeted therapies ineffective.[12–14] A small subpopulation of neural stem-like cells within the tumor, called glioma stem cells (GSCs), is thought to be the source of tumor initiation and recurrence.[15] GSCs have been shown to act as a driving factor in radio- and chemoresistance via activation of pathways involved in DNA damage response and/or repair.[16,17] MES GSCs display a more aggressive phenotype and increased radio/chemoresistance compared to other subtypes.[18,19] PN GSCs may acquire therapeutic resistance and more aggressive characteristics by shifting their phenotype and genotype toward a MES state, similar to the well-characterized epithelial–mesenchymal transition.[20] In GBM, this phenotypic transition, resulting in therapeutic resistance and poor patient prognosis, is promoted by nuclear factor-κB (NF-κB) activation.[18,21,22] The activation of several oncogenic transcription factors including signal transducer and activator of transcription 3 (STAT3) and release of pro-inflammatory cytokines is promoted by aberrant NF-κB signaling.[18] Notably, STAT3 signaling is a crucial driver of MES transition and maintenance of proliferation as well as self-renewal of GSCs.[18,23,24] Interestingly, PN GSCs exposed to radiotherapy have been shown to downregulate PN-associated markers while upregulating MES-associated markers.[25]

Extracellular vesicles (EVs) are a heterogeneous group of membrane-limited vesicles characterized by their biogenesis, originating from the plasma membrane or endosome. EVs are released by most, if not all, cell types and contain active molecules such as nucleic acids, lipids, and proteins.[26,27] Based on their mode of biogenesis, EVs can be roughly divided into two main categories: microvesicles and exosomes.[26] Exosomes originate within the endosomal system, whereas microvesicles are generated by the outward budding of membrane vesicles from the cell surface.[28] In this study, we do not differentiate between exosomes and microvesicles and collectively refer to them as EVs. The lipid bilayer structure of EVs allows for protected and directed transfer of active molecules between cells and potential exertion of biological functions.[29]

In fact, EV-mediated communication is thought to be a crucial driver in tumor progression and treatment resistance. Metastatic and migratory potential of one cell can be transferred to a recipient cell via EVs.[30–32] EVs are involved in many aspects of communication between GBM cells and their microenvironment, including cell migration, reprogramming, homing, and potential protection against therapeutic agents.[33–38]

Here, we show that MES GSC derived EVs modulate migratory potential, stemness, invasiveness, proliferation, and treatment resistance of PN GSCs. We further demonstrate that EVs play a key role in GBM intratumoral heterogeneity and MES EVs increase proliferation and chemotherapeutic resistance of PN cells through NF-κB/STAT3 signaling, both in culture and in mouse patient-derived xenograft models.

2. Experimental Section

2.1. Cell Culture

Primary glioma stem cells (GSCs) were derived from resected tumor tissue of GBM patients undergoing treatment at the Massachusetts Generals Hospital (provided by Dr. Hiroaki Wakimoto) or The Ohio State University James Comprehensive Cancer Center, in accordance with the appropriate institutional review board approval. All GSC lines used in this study including proneural cells (BT07, MGG6, MGG8 and PN157) as well as mesenchymal cells (MES83 and MES326) were previously characterized.[19,22,39–42] Cells were cultured as neurospheres and maintained in Gibco Dulbecco's Modified Eagle Medium: Nutrient Mixture F-12 (Thermo Fisher Scientific) containing the following supplements: 3×10^{-3} M L-glutamine, 1:50 B27 (Life Technologies), 20 ng mL^{-1} human recombinant EGF (R&D Systems), and 20 ng mL^{-1} human recombinant bFGF-2 (Peprotech). Nanoparticle tracking analysis was performed to confirm that the cell culture medium used had no detectable amounts of EVs. Neurospheres were dissociated using Accutase (Innovative Cell Technologies) before every passage and cultured in a humidified incubator with 5% CO_2 at 37 °C. Cells were counted using a Bright-Line Hemocytometer (Sigma).

2.2. Reagents and Constructs

Recombinant human TNFα was purchased from Peprotech. Cell viability reagent alamarBlue was purchased from Thermo Fisher Scientific and used as recommended by the manufacturer. Temozolomide and PKH67 were obtained from Sigma Aldrich. C/EBPβ shRNA construct was obtained from Sigma MISSION library (TRCN0000007440) and packaged into a lentivirus vector by the MGH Vector Core Facility.

2.3. EV Concentration from Conditioned Media

EVs were isolated by differential centrifugation (DC) or size exclusion chromatography (SEC). For DC, 5×10^6 cells were seeded in four to eight 150 mm TC-treated cell culture dishes (Corning) in 20 mL supplemented EV-free neurobasal culture medium and collected 48 h later. This conditioned medium was subject to serial centrifugation steps combined with filtration: 1) 300 × *g* for 10 min at 4 °C (Thermo Scientific Sorvall Four-Place Swinging Bucket Rotor); 2) 2000 × *g* for 10 min at 4 °C (Thermo Scientific Sorvall Four-Place Swinging Bucket Rotor); 3) filtration through 0.8 μm filter (Millipore); 4) filtrate centrifuged at 100 000 *g* in 70 Ti rotor for 2 h at 4 °C in polypropylene tubes (Beckman Coulter). The resulting pellet was resuspended in cold phosphate buffered saline (PBS) (double filtered with a 0.22 μm pore size membrane syringe filter (Millipore)) and situated on ice for 30 min, leaving the initial pellet spot covered. Finally, the pellet was resuspended by trituration with a pipette, transferred into a 1.5 mL microfuge tube, and stored at –80°C.

For SEC, the conditioned medium was centrifuged at 300 × *g* for 10 min at 4 °C to remove floating cells. 12 mL of the cell-free medium was placed into a 100 kDa Amicon Filter (Millipore) and centrifuged at 5000 × *g* for 20 min in a fixed angle rotor at 4 °C. 0.5 mL of the concentrate was applied on the SEC column (qEVoriginal/70 nm, Izon) following the column equilibration procedure according to the manufacturer's protocol. The sample was eluted by addition of PBS solution (freshly double filtered through 0.22 µm Millipore filter). An Automatic Fraction Collector (Izon) was used to collect EV-relevant fractions ("EV Zone" according to manufacturer's protocol) of 500 µL. Fractions were combined and placed into a 100 kDa Amicon Filter (Millipore) and centrifuged at 5000 × *g* for 20 min at 4 °C to concentrate EVs. Samples were transferred into a 1.5 mL microfuge tube and stored at –80 °C.

2.4. EV Quantification

EV concentration and size was analyzed by means of NanoSight LM10 instrument (Malvern, Framingham, MA) equipped with an AVT MARLIN F-033B IRF camera (Allied Vision Technologies) and NTA 3.1 Build 3.1.46 software. All nanoparticle tracking analyses were carried out with identical experiment settings (Camera Level = 12, Detection Threshold = 4). Particles were measured for 30 s, and for optimal results, EV concentrations were adjusted to obtain ≈50 EVs per field of view. Each sample was imaged in at least 5 technical replicates.

2.5. EV Treatment

PN GSCs were treated with 2×10^{10} EVs mL^{-1} (unless otherwise specified) derived with either DC or SEC every other day over eight days unless otherwise specified. For quantitative reverse transcription polymerase chain reaction (qRT-PCR) experiments, GSCs were treated with 2×10^{10} EVs mL^{-1} and incubated for 24 h before RNA extraction. For Western blot experiments, GSCs were treated with 2×10^{10} EVs mL^{-1} for two days before protein isolation. Experiments depicted in Figures 2F and 4G were performed with SEC EVs; remaining experiments were conducted using DC EVs.

2.6. In Vitro EV Uptake Experiment

BT07 GSCs expressing mCherry and MES83 GSCs expressing palmGFP (thereby labeling the EV surface[43]) were dissociated and cocultured in supplemented neurobasal medium (as described above). Cocultured sphere formation and EV uptake was monitored using a Keyence Fluorescence BZ-X800 inverted microscope. For PKH67-labelled EV uptake experiments, MGG8 GSCs were incubated with 10 ng μL^{-1} of PKH67-labelled (following manufacturer's instructions) EVs derived from MES83 GSCs. Twenty-four hours later, cells were washed with PBS before fluorescence analysis using a Nikon eclipse TE2000-U inverted microscope.

2.7. Electron Microscopy

EVs were isolated by differential centrifugation, resuspended in 20 µL double-filtered PBS and kept at 4 °C for further processing as described.[44] Briefly, an equal volume of 4% paraformaldehyde (PFA) was added to the EV sample and incubated for 2 h and 3 µL of each EV solution was applied onto grids and incubated in 2% PFA for 20 min. Sample were then transferred to a wax strip, washed with PBS, incubated in 50×10^{-3} M glycine/PBS for 5 min and blocked in 5% bovine serum albumin (BSA)/(PBS) for 10 min. Samples were then washed with PBS and incubated with 1% glutaraldehyde for 5 min. After several wash steps with H_2O, the grids were incubated in uranyl oxalate for 5 min and in 1% methyl cellulose:4% uranyl acetate (9:1) for 10 min on ice. Excess liquid was removed, and the grids were air-dried for 5–10 min. EVs were analyzed using a JEOL 1100 transmission electron microscope (JEOL, Peabody, MA) at 60 kV, and images were obtained with an AMT digital camera (Advanced Microscopy Techniques, Woburn, MA).

2.8. Scratch Assay

A scratch assay was performed to assess the migratory potential of EV treated cells as previously described.[22,45] In brief, EV treated GSCs cultured in the presence of 0.025 mg mL^{-1} Synthemax II-SC substrate (Corning) to induce a monolayer were scratched using a pipette tip to create a wound. Medium was immediately refreshed and 2×10^{10} mL^{-1} EVs were added. Cells migrating from the leading edge were photographed at different time points using phase-contrast microscopy. Distance was measured in 10× field using ImageJ (National Institutes of Health).

2.9. Sphere Formation Assay

EV treated GSCs were dissociated and different number of cells were seeded into a 96-well plate in 6 replicates. After 10 days, neurospheres of >50 µm in diameter were counted.

2.10. 3D Tumor Sphere Invasion Assay

GSCs were dissociated and treated with 2×10^{10} EVs mL^{-1} for 2 days. Equally sized tumor spheres were transferred into a 96 well plate and embedded in Corning Matrigel. Spheres were imaged 1, 4, and 21 h post seeding. Sphere invasion was analyzed with ImageJ (National Institutes of Health) and normalized to timepoint 1h (initial sphere size).[46]

2.11. TMZ Resistance Assay

GSCs were treated with EVs every other day for 8 days with 2×10^{10} EVs mL^{-1}. These cells were then seeded in 96-well plates (3×10^3 cells per well), treated with the indicated dose of TMZ and cell viability was assessed 72 h later with alamarBlue (following the manufacturer's protocol).

2.12. Radiotherapy Resistance Assay

GSCs were treated once with 2×10^9 EVs (Figure 2F) or every other day for 8 days. Treated cells were subjected to different doses of ionizing radiation and seeded in 96-well plates (3×10^3 cells per well) and cell viability was assessed 6 days later with alamarBlue.

2.13. In Vivo Orthotopic GSCs Model

All animal experiments were approved by the Massachusetts General Hospital Subcommittee on Research Animal Care and complied with guidelines set forth by the National Institutes of Health Guide for the Care and Use of Laboratory Animals. For the coinjection experiment, 5×10^4 of either MES83-Fluc or PN157-Gluc cells, or a mixture of 2.5×10^4 cells of each cell line were stereotactically implanted in 2 µL PBS using a 30-gauge Hamilton syringe into the left forebrain of nude mice (2.5 mm lateral and 0.5 mm anterior to bregma, at a 2.5 mm depth from the skull surface). For ex vivo EV modulation experiments, 3×10^4 MGG8-Fluc GSCs or the same cells treated with MES83 EVs were stereotactically implanted in the brain of mice as above. Tumor growth was monitored by Fluc and/or Gluc bioluminescence imaging using a Xenogen IVIS 200 Imaging System (PerkinElmer), after intraperitoneal (i.p.) injection of D-luciferin (150 mg kg^{-1} body weight; Gold Biotech, St. Louis, MO) for Fluc imaging or retro-orbital injection of coelenterazine (5 mg kg^{-1} body weight; Nanolight) for Gluc imaging.[47] Image intensity was quantified using Living Image software 4.3.1 (PerkinElmer).

2.14. RNA Isolation and Quantitative Real-Time PCR (q-PCR)

Cells were lysed and RNA was extracted using the RNeasy mini kit (Qiagen) followed by cDNA synthesis using 5× All-In-One RT MasterMix kit (abm). Expression of different genes was analyzed by quantitative real-time PCR using specific primers, with GAPDH and/or ACTB as an internal control (in triplicates) using a QuantStudio 3 PCR system (Applied Biosystems). The expression of various human genes analyzed in this study included: CD44, MMP2, NCAD, VIM, NESTIN, OCT4, CD133, OLIG2, SOX2, ICAM1, TNFAIP3, C/EBPβ, GAPDH, and ACTB. The sequence of all primers was obtained from the MGH primer bank (https://pga.mgh.harvard.edu/primerbank).

2.15. Western Blotting

Cell and EV pellets were suspended in RIPA buffer (Boston Bioproducts) containing 1× protease inhibitors cocktails (Boehringer Mannheim) and phosphatase inhibitors (Thermo Fisher Scientific). Thirty micrograms of protein were electrophoresed in Novex Tris-Glycine Gels (ThermoFisher), transferred to nitrocellulose membranes (Bio-Rad) followed by blocking in 5% nonfat milk in TBS/0.1% TWEEN for 1 h. Membranes were probed overnight with the primary antibody in 2.5% milk and TBS/0.1% TWEEN. The primary antibodies used were: Phospho-NF-κB p65 (Cell Signaling), NF-κB p65 (Cell Signaling), Phospho-STAT3 (Cell Signaling), STAT3 (Cell Signaling), C/EBPβ (Cell signaling), TSG101 (Abcam), Alix (Santa Cruz), Flotillin-1 (Abcam), CD44 (Cell signaling), SOX2 (Cell Signaling), GAPDH (Cell Signaling), and β-Actin (Cell Signaling). Anti-rabbit HRP-linked antibody (Cell Signaling) or anti-mouse HRP-linked antibody (Cell Signaling) corresponding to the primary antibody was used as a secondary antibody. Proteins were visualized with SuperSignal West Pico PLUS Chemiluminescent Substrate (Thermo Fisher).

2.16. NF-κB Reporter Activity

A dual secreted luciferase reporter system was used to monitor NF-κB activity as previously described.[48] Cells were cotransduced with two lentivirus vectors expressing Gaussia luciferase (Gluc) under NF-κB transcription responsive elements, as well as Vargula hilgendorfii luciferase (Vluc) under a constitutively active SV40 minimal promoter. At indicated time points, 30–50 µL aliquots of conditioned medium were collected, transferred into a 96-well white plate and assayed for Gluc and Vluc activity by adding 50 µL of either coelenterazine (20×10^{-6} M; Nanolight) or Vargulin (5 ng mL^{-1}; Nanolight) and acquiring bioluminescence signal using Synergy HTX multimode reader (Biotek).

2.17. Statistical Analysis

GraphPad Prism (v.7.0a) was used for statistical analysis of all data. Graphs and figures were generated using GraphPad Prism (v.7.0a) and Adobe Illustrator CS6. All cell culture experiments consisted of a minimum of three independent replicates and were repeated at least three times. The results are presented as the mean ± SD or SEM. Normality of distribution was verified by applying a Shapiro–Wilks test for normality. Groups with normal distribution were compared with Student's *t*-test or ANOVA. Groups with distribution deviating from normal were compared using Mann–Whitney test. Experiments involving animal survival were analyzed using a log-rank (Mantel–Cox) test and plotted as Kaplan–Meier survival curves using GraphPad Prism v.7.0a. Results were considered significant for p values < 0.05 ($*p < 0.05$; $**p < 0.01$; $***p < 0.001$).

3. Results

3.1. GSC Derived EVs Modulate Proliferation and Migratory Potential of Recipient Cells

The uptake of EVs was first confirmed by coculturing MES83 GSCs expressing palmGFP (thereby labeling secreted EV membranes[43]) with BT07 PN GSCs expressing mCherry fluorescent protein. GSC spheroids grew together to form cospheres where a dotted green fluorescent pattern on BT07 GSCs was observed, indicating potential EV exchange

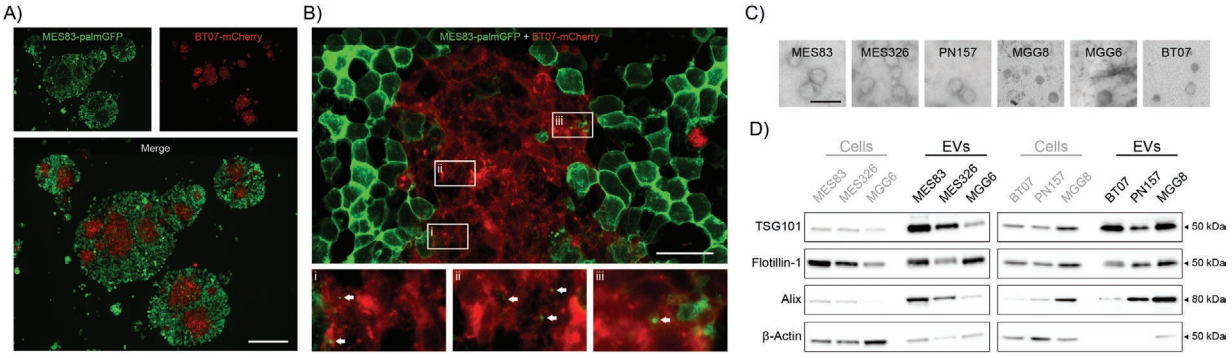

Figure 1. Visualization and characterization of GSC-derived EVs and their transfer between different GBM subtypes. A) MES83 GSCs expressing palmGFP (top left) and BT07 GSCs expressing mCherry (top right) were dissociated and cocultured, resulting in cospheres (bottom); scale bar, 500 µm. B) Dotted fluorescent pattern on BT07 GSCs indicates EV transfer from MES83 to BT07 GSCs; scale bar, 50 µm. C) Transmission electron microscopy images of MES and PN GSCs-derived EVs; scale bar, 250 nm. D) Western blot analysis for vesicle markers (TSG101, Flotillin, and ALIX) enriched in EV lysates compared to their originating cell.

(**Figure 1**A,B). Similar results were obtained when MES83 EVs were labeled with PKH67 dye and incubated with MGG8 PN GSCs, confirming sufficient EV binding/uptake in a different cell line (Figure S1A, Supporting Information). EVs released from MES and PN GSCs used in this study were then characterized. A smaller sized peak (around 70 nm) was observed after performing NTA with the control nonconditioned media. However, the detected signal does not reflect a typical EV profile and is most likely caused by small particles/protein aggregates in the media (Figure S1B, Supporting Information). While there was no significant difference in the mean particle size, MES GSCs released a higher number of EVs compared to PN GSCs (Figure S1C,D, Supporting Information). Further, the D90 diameter (defined as the diameter where 90% of the distribution has a smaller particle size and 10% has a larger particle size) of EVs derived from PN GSCs was larger compared to EVs from MES GSCs (Figure S1D,E, Supporting Information). Transmission electron microscopy images confirmed presence of EVs in all sample preparations and may indicate differences in EV morphology (Figure 1C). EV protein analysis further confirmed enrichment of vesicular protein markers (TSG 101, Flotillin-1, and ALIX) in EV samples compared to their originating cell (Figure 1D).

The modulatory effect of EVs derived from GSCs with different molecular subtypes in recipient GBM cells was then investigated. First, proliferation assays were performed in different PN recipient GSCs (MGG6, BT07) and it was observed that treatment with MES83-derived EVs increased proliferation of PN cells over time as monitored by alamarBlue and secreted Vluc reporter system (**Figure 2**A and Figure S1F–H, Supporting Information). It was asked whether EVs derived from various GSCs could further modulate the migratory potential of recipient PN cells. Utilizing a scratch wound healing assay, it was observed that PN MGG6 GSCs treated with MES83 EVs displayed a significantly greater migration potential compared to the PBS treated group, in a similar manner to control MES83 cells (Figure 2B). Interestingly, increased MGG6 migration was observed when treated with their own MGG6 PN cells. These results indicate that EVs in general, and MES83 EVs in particular, enhance migratory potential of recipient GSCs.

3.2. MES EVs Increase Stemness and Invasiveness of Recipient PN GSCs

To investigate whether EVs from a specific GSC subtype can modulate recipient GSCs, PN157 GSCs were treated with either MES83-derived EVs or PN MGG6 EVs followed by limiting dilution and sphere formation analysis. An increase in neurosphere formation was observed with recipient cells treated with MES83 EVs but not MGG6 PN EVs (Figure 2C). To elucidate the role of EVs in GSC invasiveness, a 3D tumor sphere invasion assay was performed and it was observed that MES83 EVs induced a significant increase in PN157 GSC invasiveness (Figure 2D). These results suggest that MES EVs amplify recipient GSCs self-renewal and invasion properties.

3.3. MES EVs Induce Therapeutic Resistance in PN GSCs

Since MES EVs induced self-renewal and proliferation of PN cells, it was hypothesized that MES EVs could also increase their treatment resistance. MGG6 PN GSCs were incubated with either MES83- or MGG6-derived EVs and were subjected to different doses of temozolomide (TMZ). MES83 EVs lead to an increase in TMZ resistance in recipient cells, in a similar trend to the MES83 GSC positive control (Figure 2E). Similarly, a single treatment of PN157 GSCs with MES326 EVs resulted in an increased resistance to radiation therapy (Figure 2F). These results were confirmed in different recipient PN cells (MGG8) and different MES donor cells (MES83) and EVs isolated with either DC or SEC, confirming that the observed effect is EV-specific and not related to other free proteins/contaminants obtained during DC (Figure S1I, Supporting Information). Collectively, these results show that EVs derived from MES GSCs lead to chemo- and radio-resistance in recipient PN cells.

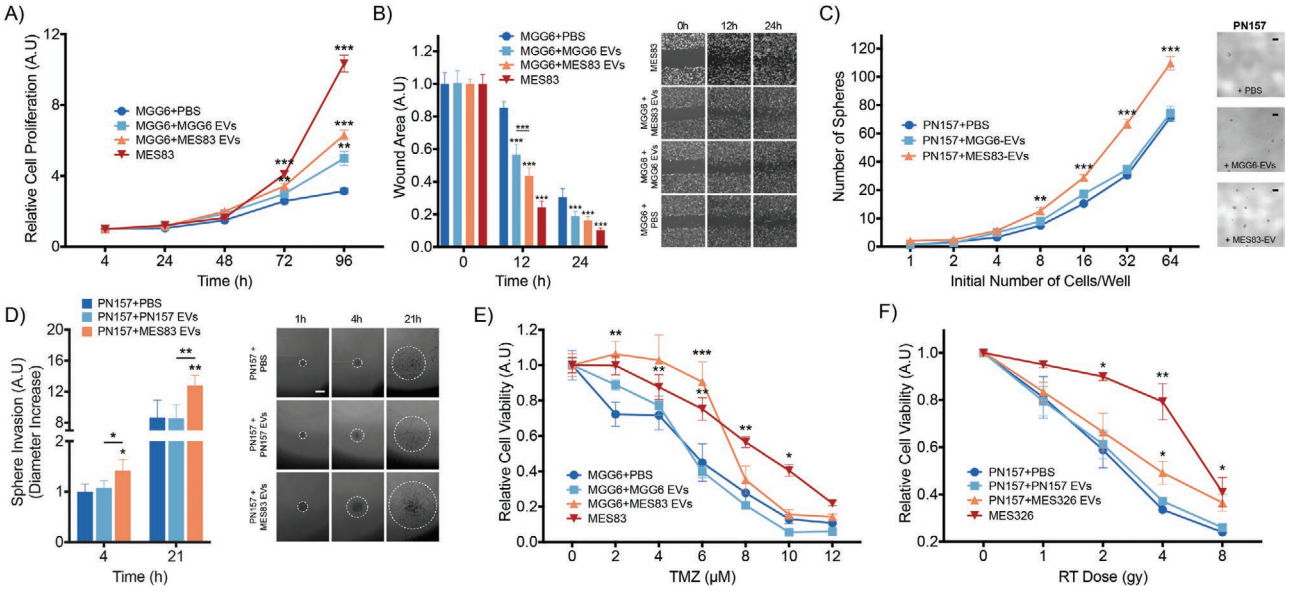

Figure 2. GSC-derived EVs modulate proliferation, migratory potential, stemness, invasiveness, and treatment resistance in recipient GSCs. A) MGG6 were treated with either MGG6 or MES83-derived EVs or PBS and cell proliferation was monitored at different time points by alamarBlue; MES83 cells were included as a positive control. B) MGG6 GSCs monolayer was treated with EVs derived from MGG6, MES83, or PBS control, scratched, and analyzed by microscopy at different time points. MES83 cells were used as a positive control. Representative images (right) and quantification of migratory cells (left) are shown. C) PN157 cells were treated with either MES83, PN MGG6-derived EVs or PBS control followed by plating different number of cells, down to a single cell, and 10 days later, spheres > 50 μm in diameter were counted. Micrographs of neurospheres are shown in the right panel; scale bar, 100 μm. D) PN157 cells were treated with either EVs derived from MES83 or PN157 or PBS control and seeded to allow sphere formation. Equally sized spheres were transferred to a Matrigel-containing 96 well plate. Sphere invasion was imaged after 1, 4, and 21 h. Micrographs of neurospheres at different time points are shown in the right panel; scale bar, 500 μm. E,F) PN GSCs were cultured with different MES GSC-derived EVs and treated with different doses of E) temozolomide or F) ionizing radiation and cell viability was analyzed 3 or 6 days later, respectively; $*p < 0.05$; $**p < 0.01$; $***p < 0.001$ as analyzed by ANOVA ($n \geq 3$).

3.4. MES Cells Modulate Growth of PN Cells and Mouse Survival in Patient-Derived Xenograft Models

To corroborate the data observed in culture, the influence of MES cells/EVs was evaluated on PN cell growth in vivo using dual bioluminescence imaging. 5×10^4 GSCs of either PN157-Fluc cells, MES83-Gluc cells, or a mixture of 2.5×10^4 of each GSCs were stereotactically implanted (**Figure 3**A). Bioluminescence imaging performed 14 days after implantation showed that PN cells, when coinjected with MES cells, exhibited a significantly increased Fluc signal and therefore PN tumor growth, compared to PN cells implanted alone. The average Fluc activity in PN cells (normalized to implanted cell number) was around 7-fold higher when coinjected with MES cells compared to PN cells implanted alone ($p = 0.0047$, $n = 6$ per group; Figure 3B). On the other hand, no significant change in Gluc signal was observed in MES cells injected alone or together with PN cells (Figure 3C). Further, and as expected, mice implanted with PN tumors exhibited a significantly longer survival compared to their MES counterparts ($n = 6$ per group; $p = 0.0007$; Figure 3D). Interestingly, mice injected with a mixture of PN and MES cells showed a very similar survival rate (with no significant difference) compared to mice injected with MES cells alone ($p = 0.1732$ MES + PN vs MES cells; $p = 0.007$ MES + PN vs PN cells; Figure 3D).

3.5. EVs Modulate Growth and Therapeutic Resistance of GSCs in Patient-Derived Xenograft Models

To confirm that the observed enhanced PN tumor proliferation is mediated by EVs, MGG8-Fluc PN GSCs were preheated with MES83 EVs (every other day for 8 days) ex vivo and then implanted into the brain of mice. Again, a significant increase in tumor growth was observed in PN GSCs pretreated with MES EVs compared to control. At day 30, the average relative median Fluc activity in PN cells pretreated with MES EVs was around 10-fold higher compared to control PN tumors ($n = 7$ per group, $p = 0.0013$; Figure 3E).

To confirm that MES EVs lead to therapeutic resistance in vivo, the same experiment was repeated above where PN cells were pretreated with MES EVs and injected in the brain of mice. Once tumor reached a significant size, each group was divided into 2 subgroups ($n = 5$ per group) where one subgroup was treated with TMZ (5 mg kg^{-1} body weight daily over 5 days) while the other group received a vehicle control. Although TMZ treatment leads to a significant decrease in tumor volume in both groups ($p = 0.0256$ MGG8 + PBS CTRL vs MGG8 + PBS TMZ; $p = 0.0470$ MGG8 + PBS CTRL vs MGG + MES83 EVs TMZ) (Figure 3F), the PN GSCs tumors precultured with MES EVs showed reduced response to TMZ therapy. In addition, TMZ led to a significant increase in mouse survival in both groups ($p = 0.0018$ MGG8 + PBS CTRL vs MGG8 + PBS TMZ;

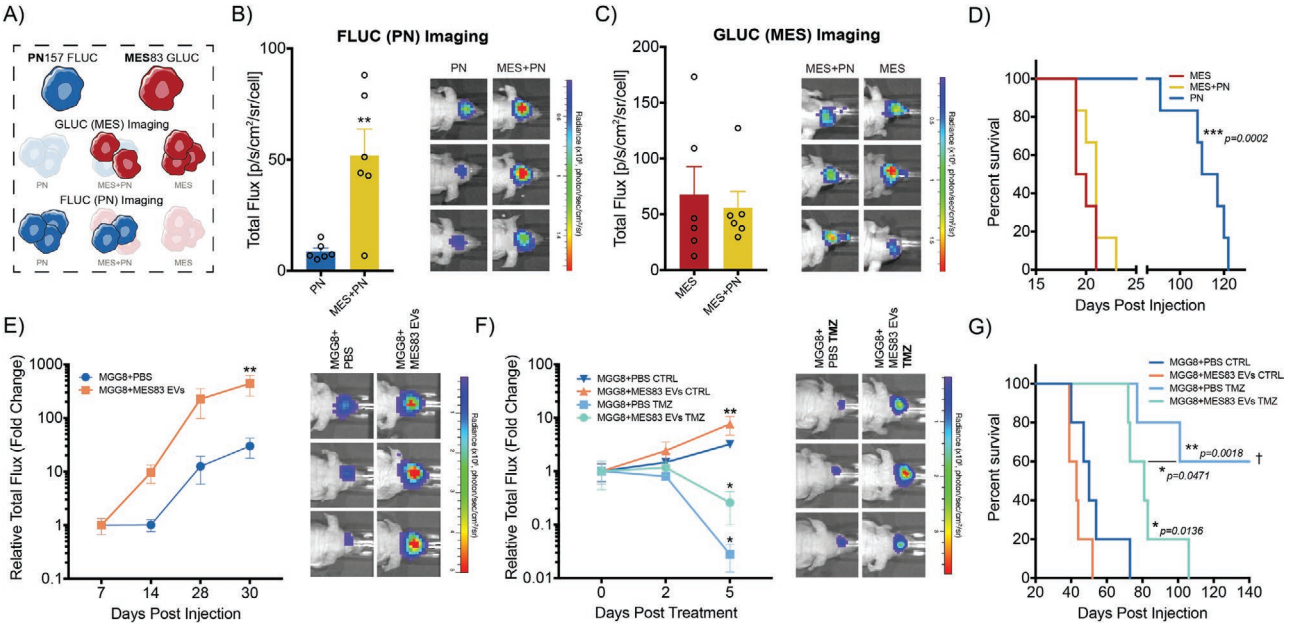

Figure 3. MES EVs increase PN cells proliferation and treatment resistance in patient-derived xenograft models. A) Workflow depicting labeling and coinjection of PN and MES GSCs. PN157-Fluc, MES83-Gluc, or a combination of both GSCs were implanted in the brain of mice. Tumor growth for each cell population was monitored by dual Fluc and Gluc bioluminescence imaging. B) Representative Fluc (PN cells) bioluminescence images of mice from each group at 2 weeks post-injection is shown (right) and tumor-associated signal is quantified (left); $^{**}p = 0.0047$, *t*-test (two-tailed); $n = 6$). C) Representative Gluc (MES cells) bioluminescence images of mice from each group at 2 weeks post-injection is shown (right), and tumor-associated signal is quantified (left); $p = 0.8182$, Mann–Whitney test; $n = 6$). D) Kaplan–Meier survival curves for each group in (B) and (C) ($p = 0.0007$ MES vs PN cells; $p = 0.1732$ MES + PN vs. MES cells; $p = 0.0007$ MES + PN vs. PN cells; log-rank (Mantel–Cox) test; $n = 6$ per group). E) MGG8-Fluc cells were pretreated with MES83-derived EVs or PBS and implanted in the brain of mice. Tumor growth was monitored by Fluc imaging. Representative bioluminescence images of mice from each group at day 30 postinjection are shown (right) and tumor-associated signal is quantified and normalized where signals 2 weeks postinjection are set at 1 (left); $^{**}p = 0.0013$ Mann–Whitney test; $n = 7$ per group; F) The same experiment as in (D) was performed but at day 27, each group of mice was divided in 2 different subgroups which either received TMZ or vehicle control and response to therapy was monitored by Fluc imaging. Representative bioluminescence images of mice from each TMZ-treated group at day 31 postimplantation (or day 5 post-treatment) is shown (right) and tumor-associated signal is quantified and normalized where signals before treatment are set at 1 (left); $p = 0.0024$ MGG8 + PBS CTRL versus MGG8 + MES83 EVs CTRL; $p = 0.0470$ MGG8 + PBS CTRL versus MGG8 + MES83 EVs TMZ; $p = 0.0256$ MGG8 + PBS CTRL versus MGG8 + PBS TMZ; ANOVA; $n = 5$ per group). G) Kaplan–Meier survival curves for each group in (F); $p = 0.1107$ MGG8 + PBS CTRL versus MGG8 + MES83 EVs CTRL; $p = 0.0136$ MGG8 + PBS CTRL versus MGG8 + MES83 EVs TMZ; $p = 0.0018$ MGG8 + PBS CTRL versus MGG8 + PBS TMZ; $p = 0.0471$ MGG8 + PBS TMZ versus MGG8 + MES83 EVs TMZ; Log-rank (Mantel–Cox) test; $n = 5$) ($^{*}p < 0.05$, $^{**}p < 0.01$, $^{***}p < 0.001$).

$p = 0.0136$ MGG8 + PBS CTRL vs MGG + MES83 EVs TMZ). Importantly, mice bearing PN GSCs precultured with MES EVs showed a significant decrease in mouse survival compared to PN cells precultured with PBS, both treated with TMZ. Three out of five mice from the MGG8 + PBS TMZ group survived 140 days post injection, but all mice from the MGG8 + MES EV TMZ group died by day 105 (median survival for MGG8 + PBS TMZ is 141 days vs 81 days for MGG8 + MES EV TMZ; $p = 0.0471$; Figure 3G).

Altogether, the results suggest that EVs derived from the more aggressive MES GSCs can modulate PN GSCs, leading to an increase in their proliferation and resistance to radio- and chemotherapy.

3.6. MES EVs Promote GSCs Aggressiveness and Mesenchymal Transition through NF-κB/STAT3 Signaling

The results showed that EVs derived from MES GSCs lead to increased aggressiveness and therapeutic resistance, features of the mesenchymal GBM subtype. It was therefore evaluated whether EVs induce mesenchymal transition in recipient cells. Indeed, PN GSCs treated with EV-derived from MES GSCs showed increased expression of MES Markers (CD44, MMP2, NCAD and VIM) and stemness markers (Nestin, OCT-4) as analyzed by qRT-PCR (**Figure 4**A,C). Interestingly, MES EVs lead to a decrease in PN markers (CD133, Olig2 and SOX2) in recipient cells (Figure 4B). Surprisingly, EVs derived from PN cells had no effect on MES or PN markers but lead to a decrease in stemness marker OCT-4 in recipient PN cells (Figure 4A–C). These results were reproducible in a different PN recipient cell line (PN157; Figure 2A, Supporting Information) and confirmed by Western blotting in 2 PN cells (MGG8 and BT07; Figure 4D). Interestingly, EV protein content analysis revealed presence of CD44 in MES cells and their corresponding EVs but not in PN cells or their EVs, while SOX2 is only expressed in PN GSCs but does not appear to be significantly packaged in their EVs (Figure 4E).

The NF-κB pathway plays an essential role in MES transition and acquired tumor treatment resistance in GBM.[49–51]

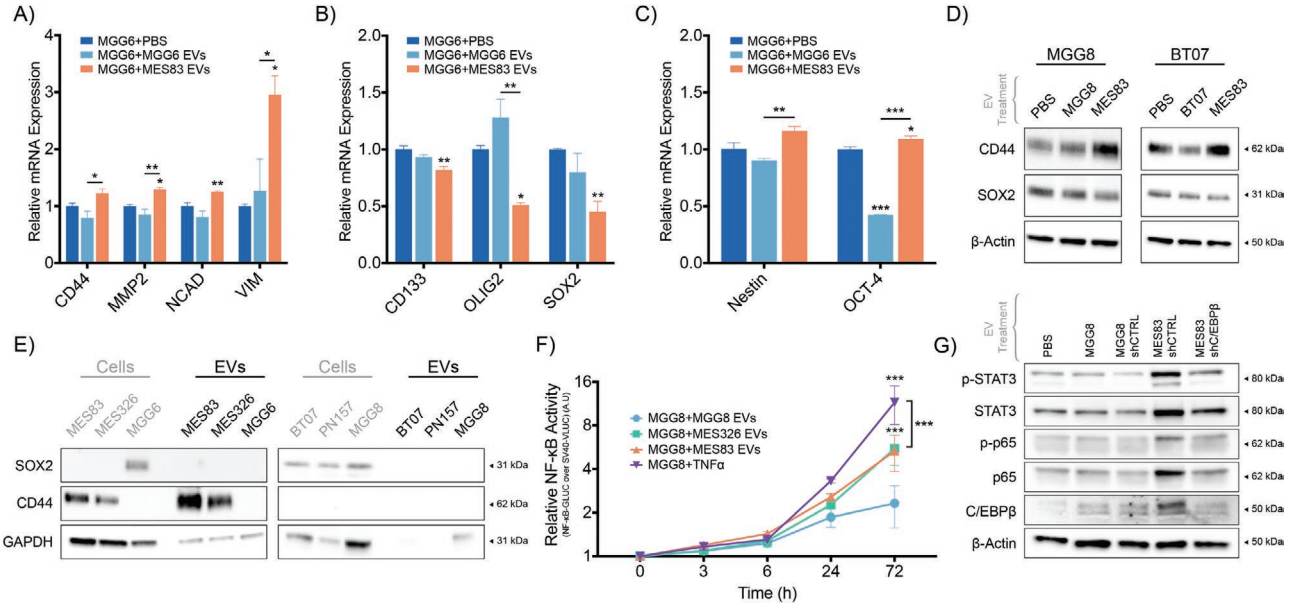

Figure 4. EVs induce mesenchymal transition through NF-κB/STAT3 signaling in recipient PN cells. A–C) MGG6 PN GSCs were treated with EV-derived from either MGG6 or MES83 GSCs for 24 h and analyzed by qRT-PCR for different A) mesenchymal, B) PN, and C) stemness markers. D) Different PN cell lines (MGG8 and BT07) were treated with PBS or EVs collected from MGG8, BT07, or MES83 GSCs. Cell lysates were analyzed by Western blotting for CD44, SOX2 and β-actin loading control. E) Cell and EV lysates were analyzed by Western blotting for SOX2, CD44 and GAPDH loading control. F) Time-dependent NF-κB-Gluc activity (normalized to SV40-Vluc internal control) in MGG8 GSCs treated with TNFα (5 ng mL^{-1}), MGG8 EVs, MES326 EVs, or MES83 EVs. G) MGG8 PN GSCs were treated with PBS or EVs collected from MGG8, MGG8 cells expressing scrambled shRNA control (MGG8 shCTRL), MES83 expressing shCTRL (MES83 shCTRL), or MES83 expressing shRNA against C/EBPβ (shC/EBPβ). Cell lysate was analyzed by Western blotting for p-STAT3, STAT3, p-p65, p65, C/EBPβ, and β-actin loading control. ANOVA (*$p < 0.05$; **$p < 0.01$; ***$p < 0.001$; $n \geq 3$).

Interestingly, a significant increase in mRNA expression of NF-κB target genes (TNFAIP3, ICAM1) was detected 24 h after post-treatment with MES EVs in different PN GSC lines (PN157, MGG6, MGG8, BT07; Figure S2B, Supporting Information), and this increase appears to be dose-dependent, with the most significant effect after addition of 2–4 × 10^{10} EVs mL^{-1} (Figure S2C,D, Supporting Information). These results were confirmed by an increased expression of NF-κB reporter luciferase activity over time in response to EVs from different MES donor GSCs (MES83, MES326) and in different PN recipient GSCs (PN157, BT07, MGG8; Figure 4F and Figure S2E,F, Supporting Information). Western blot analysis showed that PN cells treated with MES EVs induced increased phosphorylation of p65 (ser536), a marker for NF-κB activation (Figure 4G).

NF-κB signaling promotes the release of proinflammatory cytokines and activation of several oncogenic transcription factors.[18] Signal transducer and activator of transcription 3 (STAT 3) and CCAAT/enhancer binding protein b (C/EBPβ) are master regulators of the MES signature that act downstream of NF-κB.[24,52] Western blot analysis on PN MGG8 cells treated with MES83 EVs (collected by SEC) revealed that increased phosphorylated-p65 coincided with increased levels of phosphorylated-STAT3 (pSTAT3) and C/EBPβ (Figure 4G). Importantly, knockdown of C/EBPβ in the MES donor GSCs prior to EV concentration and treatment reversed phosphorylation of p65 and STAT3 as well as decreased C/EBPβ levels in recipient PN cells. These findings suggest that MES EVs upregulate NF-κB and STAT3 activity in recipient PN cells through C/EBPβ, pointing to the causal mechanism that may be involved in EV-mediated MES transition and therapeutic resistance.

Altogether, the findings show that MES GSCs release EVs which are then taken up by PN cells, leading to their enhanced stemness, proliferation, migratory potential, invasiveness, and therapeutic resistance through NF-κB/STAT3 mediated mesenchymal transition.

4. Discussion

Extracellular vesicle-mediated cell communication within the tumor or its microenvironment has been shown to be a crucial driver of tumor invasion, migration, progression, and therapeutic resistance.[33–38] We focused our study on the role of EVs within the different GSC populations/subtypes in glioblastoma (GBM). We showed that EVs secreted from GSCs with the aggressive mesenchymal subtype could modulate GSCs with the PN subtype by inducing mesenchymal transition, thereby increasing migratory potential, stemness, invasiveness, proliferation as well as chemo- and radiotherapeutic resistance within the same tumor. Our results underline the role of EVs in maintaining intratumoral heterogeneity in different cancers, including GBM.[38]

We add new insights in the role of EVs in GSC plasticity by demonstrating that PN GSCs treated with EVs from MES cells exhibit a shift toward a mesenchymal state through NF-κB/STAT3 signaling. Tumor-derived EVs carry a pro-epithelial to mesenchymal transition program that enhances the invasive

and migratory capabilities of recipient cells and contributes to premetastatic niche formation.[53] In GBM specifically, a shift from a PN to a MES subtype can occur and is commonly observed in patients following radiation therapy and chemotherapy during recurrence.[54] Unbiased interrogation of a glioma-specific regulatory network revealed that two transcription factors, STAT3 and C/EBPβ, act as synergistic initiators and master regulators of MES transition.[24] Abnormal coexpression of STAT3 and C/EBPβ reprograms neural stem cells along the aberrant MES lineage.[24] Elimination of these two factors in glioma cells led to a collapse of the MES signature, thereby reducing tumor aggressiveness.[24] Minata et al. demonstrated that C/EBPβ, but not STAT3, is responsible for the ionizing radiation-induced shift to MES signature in PN cells.[25] We showed that EVs from MES GSCs induce mesenchymal transition in recipient PN cells through an increase in activation of NF-κB/STAT3 signaling, mediated by C/EBPβ. Clinically, our data may provide the rationale to inhibit EV release, interfere with selective EV uptake, or use inhibitors of NF-κB or STAT3 to hinder MES transition. Targeting intratumoral EV crosstalk may reduce protumoral effects of EVs and subsequent GBM aggressiveness and recurrence.

Although we demonstrate that EVs derived from C/EBPβ-deprived MES cells reverses activation of NF-κB/STAT3 in recipient PN cells, other EV cargo composites may also be involved in this acquired aggressiveness and treatment resistance in recipient cells. Interestingly, the content of EVs mirrors the phenotypic signature of corresponding secreting GSCs, allowing potential development of biomarkers for GBM subtyping.[38,55] Further, mRNA expression profiles reflective of TMZ resistance are also mirrored in the transcriptome of their corresponding EVs.[56] Additional studies are needed to investigate the exact molecular makeup of MES GSC derived EVs and especially their mesenchymal transition inducing content. Earlier findings have shown that EVs transfer of p-STAT3 promotes resistance to 5-fluorouracil (5-FU) in colorectal cancer cells.[57] A similar mechanism could be responsible for the STAT3/NF-κB activation and resulting mesenchymal transition in GBM since we also see increased p-STAT3 levels in recipient cells. Further, apoptotic GBM cells undergoing therapy secrete EVs loaded with components of spliceosomes, thereby altering RNA splicing in recipient surviving tumor cells, leading to a more aggressive phenotype and eventual therapeutic resistance.[58] External stimuli from the tumor microenvironment play a pivotal role in PMT.[59] GSCs can acquire mesenchymal features upon stimulation by secretory cytokines such as TGF-β.[60] Epigenetic regulation by histone modification, DNA methylation, and chromatin remodeling is an additional mechanism by which GBM cells can undergo malignant transformation.[61,62] Furthermore, miRNAs and long noncoding RNAs have been shown to play an essential role in GBM pathogenesis and mesenchymal transition.[63–66] It would be interesting to evaluate all of these events in the context of EVs and whether some of these factors are also responsible for the phenotypic switch observed during cellular EV exchange.

The EV concentration used in this study is based on dose escalation analyses where PN GSCs were treated with different concentrations of MES EVs followed by the evaluation of various mesenchymal markers. Under our assay conditions, the most significant effect was observed after addition of $2–4 \times 10^{10}$ EVs mL^{-1} and therefore this concentration range was used throughout the study. The actual in vivo EV exposure may be different as cells continuously secrete and exchange EVs. At this point, it is technically challenging to evaluate the exact number of EVs secreted by any given cell. Future studies may overcome this challenge as more accurate and reliable EV quantification and imaging methods evolve.

In summary, we show that EVs play a crucial role in maintaining intratumoral heterogeneity and GBM plasticity by changing the phenotypic behavior and transcriptomic composition of recipient GSCs, mirroring characteristics of EV donor cells, and leading to therapeutic resistance through NF-κB/STAT3 signaling.

Supporting Information

Supporting Information is available from the Wiley Online Library or from the author.

Acknowledgements

M.W.S. and M.L. contributed equally to this work. This work was supported by grants from the National Institutes of Health, the National Cancer Institute 2P01CA069246 (BAT/AC), and the National institute of Neurological disorders and Stroke R01NS064983 (BAT). The authors would like to acknowledge Dr. Marian DiFiglia and Ellen Sapp (Massachusetts General Hospital) for EM image acquisition, and Ziyi Liu for producing the viral vector in the MGH vector core (supported by NIH/NINDS P30NS04776) as well as 1S10RR025504 Shared Instrumentation grant for the IVIS imaging system. Furthermore, the authors would like to thank Dr. Xandra Breakefield, Dr. Pike See Cheah, and Dr. Killian O'Brien for their valuable help with EV profile interpretation. The authors also thank Dr. Hiroaki Wakimoto (Massachusetts General Hospital) for providing some of the GSCs used in this study.

Conflict of Interest

The authors declare no conflict of interest.

Keywords

extracellular vesicles, glioblastoma, mesenchymal transition, NF-κB signaling, STAT3 signaling, treatment resistance

Received: December 31, 2019
Revised: May 23, 2020
Published online:

[1] Q. T. Ostrom, H. Gittleman, J. Fulop, M. Liu, R. Blanda, C. Kromer, Y. Wolinsky, C. Kruchko, J. S. Barnholtz-Sloan, *Neuro-Oncology* **2015**, *17*, 624.
[2] Y. P. Ramirez, J. L. Weatherbee, R. T. Wheelhouse, A. H. Ross, *Pharmaceuticals* **2013**, *6*, 1475.
[3] R. Stupp, W. P. Mason, M. J. van den Bent, M. Weller, B. Fisher, M. J. B. Taphoorn, K. Belanger, A. A. Brandes, C. Marosi,

U. Bogdahn, J. Curschmann, R. C. Janzer, S. K. Ludwin, T. Gorlia, A. Allgeier, D. Lacombe, J. G. Cairncross, E. Eisenhauer, R. O. Mirimanoff, *N. Engl. J. Med.* **2005**, *352*, 987.

[4] W. Wick, T. Gorlia, M. Bendszus, M. Taphoorn, F. Sahm, I. Harting, A. A. Brandes, W. Taal, J. Domont, A. Idbaih, M. Campone, P. M. Clement, R. Stupp, M. Fabbro, E. Le Rhun, F. Dubois, M. Weller, A. von Deimling, V. Golfinopoulos, J. C. Bromberg, M. Platten, M. Klein, M. J. van den Bent, *N. Engl. J. Med.* **2017**, *377*, 1954.

[5] C. Fernandes, A. Costa, L. Osório, R. C. Lago, L. Paulo, C. Bruno, C. Cláudia, *Glioblastoma*, Codon Publications, Brisbane, AU **2017**, pp. 197–241.

[6] C. W. Brennan, R. G. W. Verhaak, A. McKenna, B. Campos, H. Noushmehr, S. R. Salama, S. Zheng, D. Chakravarty, J. Z. Sanborn, S. H. Berman, R. Beroukhim, B. Bernard, C.-J. Wu, G. Genovese, I. Shmulevich, J. Barnholtz-Sloan, L. Zou, R. Vegesna, S. A. Shukla, G. Ciriello, W. K. A. Yung, W. Zhang, C. Sougnez, T. Mikkelsen, K. Aldape, D. D. Bigner, E. G. Van Meir, M. Prados, A. E. Sloan, K. L. Black et al., *Cell* **2013**, *155*, 462.

[7] B. S. Melin, J. S. Barnholtz-Sloan, M. R. Wrensch, C. Johansen, D. Il'yasova, B. Kinnersley, Q. T. Ostrom, K. Labreche, Y. Chen, G. Armstrong, Y. Liu, J. E. Eckel-Passow, P. A. Decker, M. Labussière, A. Idbaih, K. Hoang-Xuan, A. L. Di Stefano, K. Mokhtari, J. Y. Delattre, P. Broderick, P. Galan, K. Gousias, J. Schramm, M. J. Schoemaker, S. J. Fleming, S. Herms, S. Heilmann, M. M. Nöthen, H. E. Wichmann, S. Schreiber et al., *Nat. Genet.* **2017**, *49*, 789.

[8] D. W. Parsons, S. Jones, X. Zhang, J. C. H. Lin, R. J. Leary, P. Angenendt, P. Mankoo, H. Carter, I. M. Siu, G. L. Gallia, A. Olivi, R. McLendon, B. A. Rasheed, S. Keir, T. Nikolskaya, Y. Nikolsky, D. A. Busam, H. Tekleab, L. A. Diaz, J. Hartigan, D. R. Smith, R. L. Strausberg, S. K. N. Marie, S. M. O. Shinjo, H. Yan, G. J. Riggins, D. D. Bigner, R. Karchin, N. Papadopoulos, G. Parmigiani, B. Vogelstein, V. E. Velculescu, K. W. Kinzler, *Science* **2008**, *321*, 1807.

[9] R. P. Pangeni, Z. Zhang, A. A. Alvarez, X. Wan, N. Sastry, S. Lu, T. Shi, T. Huang, C. X. Lei, C. D. James, J. A. Kessler, C. W. Brennan, I. Nakano, X. Lu, B. Hu, W. Zhang, S. Y. Cheng, *Epigenetics* **2018**, *13*, 432.

[10] Q. Wang, B. Hu, X. Hu, H. Kim, M. Squatrito, L. Scarpace, A. C. DeCarvalho, S. Lyu, P. Li, Y. Li, F. Barthel, H. J. Cho, Y.-H. Lin, N. Satani, E. Martinez-Ledesma, S. Zheng, E. Chang, C.-E. G. Sauvé, A. Olar, Z. D. Lan, G. Finocchiaro, J. J. Phillips, M. S. Berger, K. R. Gabrusiewicz, G. Wang, E. Eskilsson, J. Hu, T. Mikkelsen, R. A. DePinho, F. Muller, A. B. Heimberger, E. P. Sulman, D.-H. Nam, R. G. W. Verhaak, *Cancer Cell* **2017**, *32*, 42.

[11] A. P. Patel, I. Tirosh, J. J. Trombetta, A. K. Shalek, S. M. Gillespie, H. Wakimoto, D. P. Cahill, B. V. Nahed, W. T. Curry, R. L. Martuza, D. N. Louis, O. Rozenblatt-Rosen, M. L. Suva, A. Regev, B. E. Bernstein, M. L. Suvà, A. Regev, B. E. Bernstein, *Science* **2014**, *344*, 1396.

[12] J. J. Parker, P. Canoll, L. Niswander, B. K. Kleinschmidt-DeMasters, K. Foshay, A. Waziri, *Sci. Rep.* **2018**, *8*, 18002.

[13] N. R. Parker, P. Khong, J. F. Parkinson, V. M. Howell, H. R. Wheeler, *Front. Oncol.* **2015**, *5*, https://doi.org/10.3389/fonc.2015.00055.

[14] M. A. Qazi, P. Vora, C. Venugopal, S. S. Sidhu, J. Moffat, C. Swanton, S. K. Singh, *Ann. Oncol.* **2017**, *28*, 1448.

[15] J. D. Lathia, S. C. Mack, E. E. Mulkearns-Hubert, C. L. L. Valentim, J. N. Rich, *Genes Dev.* **2015**, *29*, 1203.

[16] S. Bao, Q. Wu, R. E. McLendon, Y. Hao, Q. Shi, A. B. Hjelmeland, M. W. Dewhirst, D. D. Bigner, J. N. Rich, *Nature* **2006**, *444*, 756.

[17] J. Chen, Y. Li, T. S. Yu, R. M. McKay, D. K. Burns, S. G. Kernie, L. F. Parada, *Nature* **2012**, *488*, 522.

[18] K. P. L. L. Bhat, V. Balasubramaniyan, B. Vaillant, R. Ezhilarasan, K. Hummelink, F. Hollingsworth, K. Wani, L. Heathcock, J. D. James, L. D. Goodman, S. Conroy, L. Long, N. Lelic, S. Wang, J. Gumin, D. Raj, Y. Kodama, A. Raghunathan, A. Olar, K. Joshi, C. E. Pelloski, A. Heimberger, S. H. Kim, D. P. Cahill, G. Rao, W. F. A. DenDunnen, H. W. G. M. G. M. Boddeke, H. S. Phillips, I. Nakano, F. F. Lang, H. Colman, E. P. Sulman, K. Aldape, W. F. A. A. Den Dunnen, H. W. G. M. G. M. Boddeke, H. S. Phillips, I. Nakano, F. F. Lang, H. Colman, E. P. Sulman, K. Aldape, *Cancer Cell* **2013**, *24*, 331.

[19] M. Wang, P. Li, P. V. Benos, L. Santana-Santos, S. Luthra, J. Li, B. B. Hu, S.-Y. Cheng, L. Smith, I. Nakano, R. W. Sobol, S.-H. Kim, U. R. Chandran, K. Joshi, P. Mao, K. Joshi, J. Li, S.-H. Kim, P. Li, L. Santana-Santos, S. Luthra, U. R. Chandran, P. V. Benos, L. Smith, M. Wang, B. B. Hu, S.-Y. Cheng, R. W. Sobol, I. Nakano, *Proc. Natl. Acad. Sci. USA* **2013**, *110*, 8644.

[20] A. Dongre, R. A. Weinberg, *Nat. Rev. Mol. Cell Biol.* **2019**, *20*, 69.

[21] C. C. da Hora, K. Pinkham, L. Carvalho, M. Zinter, E. Tabet, I. Nakano, B. A. Tannous, C. E. Badr, *Cell Death Discovery* **2019**, *5*, 72.

[22] J. Teng, C. C. Da Hora, R. S. Kantar, I. Nakano, H. Wakimoto, T. T. Batchelor, E. Antonio Chiocca, C. E. Badr, B. A. Tannous, *NeuroOncology* **2017**, *19*, 820.

[23] M. M. Sherry, A. Reeves, J. K. Wu, B. H. Cochran, *Stem Cells* **2009**, *27*, 2383.

[24] M. S. Carro, W. K. Lim, M. J. Alvarez, R. J. Bollo, X. Zhao, E. Y. Snyder, E. P. Sulman, S. L. Anne, F. Doetsch, H. Colman, A. Lasorella, K. Aldape, A. Califano, A. Iavarone, *Nature* **2010**, *463*, 318.

[25] M. Minata, A. Audia, J. Shi, S. Lu, J. Bernstock, M. S. Pavlyukov, A. Das, S. H. Kim, Y. J. Shin, Y. Lee, H. Koo, K. Snigdha, I. Waghmare, X. Guo, A. Mohyeldin, D. Gallego-Perez, J. Wang, D. Chen, P. Cheng, F. Mukheef, M. Contreras, J. F. Reyes, B. Vaillant, E. P. Sulman, S. Y. Cheng, J. M. Markert, B. A. Tannous, X. Lu, M. Kango-Singh, L. J. Lee, D. H. Nam, I. Nakano, K. P. Bhat, *Cell Rep.* **2019**, *26*, 1893.

[26] E. R. Abels, X. O. Breakefield, *Cell. Mol. Neurobiol.* **2016**, *36*, 301.

[27] M. P. Zaborowski, L. Balaj, X. O. Breakefield, C. P. Lai, *BioScience* **2015**, *65*, 783.

[28] G. Van Niel, G. D'Angelo, G. Raposo, *Nat. Rev. Mol. Cell Biol.* **2018**, *19*, 213.

[29] S. L. N. Maas, X. O. Breakefield, A. M. Weaver, *Trends Cell Biol.* **2017**, *27*, 172.

[30] C. E. Brown, B. Badie, M. E. Barish, L. Weng, R. Julie, W. Chang, A. Naranjo, R. Starr, J. Wagner, C. Wright, Y. Zhai, J. R. Bading, J. A. Ressler, J. Portnow, M. D. Apuzzo, S. J. Forman, M. C. Jensen, *Nature* **2015**, *21*, 4062.

[31] A. Zomer, C. Maynard, F. J. Verweij, A. Kamermans, R. Schäfer, E. Beerling, R. M. Schiffelers, E. De Wit, J. Berenguer, S. I. J. Ellenbroek, T. Wurdinger, D. M. Pegtel, J. Van Rheenen, *Cell* **2015**, *161*, 1046.

[32] J. Liao, R. Liu, Y. J. Shi, L. H. Yin, Y. P. Pu, *Int. J. Oncol.* **2016**, *48*, 2567.

[33] E. R. Abels, S. L. N. Maas, L. Nieland, Z. Wei, P. S. Cheah, E. Tai, C. J. Kolsteeg, S. A. Dusoswa, D. T. Ting, S. Hickman, J. El Khoury, A. M. Krichevsky, M. L. D. Broekman, X. O. Breakefield, *Cell Rep.* **2019**, *28*, 3105.

[34] J. Skog, T. Würdinger, S. van Rijn, D. H. Meijer, L. Gainche, W. T. Curry, B. S. Carter, A. M. Krichevsky, X. O. Breakefield, *Nat. Cell Biol.* **2008**, *10*, 1470.

[35] J. Berenguer, T. Lagerweij, X. W. Zhao, S. Dusoswa, P. van der Stoop, B. Westerman, M. C. d. Gooijer, M. Zoetemelk, A. Zomer, M. H. W. Crommentuijn, L. E. Wedekind, À. López-López, A. Giovanazzi, M. Bruch-Oms, I. H. va. der Meulen-Muileman, R. M. Reijmers, T. H. van Kuppevelt, J. J. García-Vallejo, Y. van Kooyk, B. A. Tannous, P. Wesseling, D. Koppers-Lalic, W. P. Vandertop, D. P. Noske, V. W. van Beusechem, J. van Rheenen, D. M. Pegtel, O. van Tellingen, T. Wurdinger, *J. Extracell. Vesicles* **2018**, *7*, 1446660.

[36] J. Godlewski, A. M. Krichevsky, M. D. Johnson, E. A. Chiocca, A. Bronisz, *Neuro-Oncology* **2015**, *17*, 652.
[37] K. E. Van Der Vos, E. R. Abels, X. Zhang, C. Lai, E. Carrizosa, D. Oakley, S. Prabhakar, O. Mardini, M. H. W. Crommentuijn, J. Skog, A. M. Krichevsky, A. Stemmer-Rachamimov, T. R. Mempel, J. El Khoury, S. E. Hickman, X. O. Breakefield, *Neuro-Oncology* **2016**, *18*, 58.
[38] F. Ricklefs, M. Mineo, A. K. Rooj, I. Nakano, A. Charest, R. Weissleder, X. O. Breakefield, E. A. Chiocca, J. Godlewski, A. Bronisz, *Cancer Res.* **2016**, *76*, 2876.
[39] H. Wakimoto, S. Kesari, C. J. Farrell, W. T. Curry, C. Zaupa, M. Aghi, T. Kuroda, A. Stemmer-Rachamimov, K. Shah, T. C. Liu, D. S. Jeyaretna, J. Debasitis, J. Pruszak, R. L. Martuza, S. D. Rabkin, *Cancer Res.* **2009**, *69*, 3472.
[40] H. Wakimoto, G. Mohapatra, R. Kanai, W. T. Curry, S. Yip, M. Nitta, A. P. Patel, Z. R. Barnard, A. O. Stemmer-Rachamimov, D. N. Louis, R. L. Martuza, S. D. Rabkin, *Neuro-Oncology* **2012**, *14*, 132.
[41] T. Asklund, S. Kvarnbrink, C. Holmlund, C. Wibom, T. Bergenheim, R. Henriksson, H. Hedman, *Anticancer Res* **2012**, *32*, 2407.
[42] C. C. da Hora, M. W. Schweiger, T. Wurdinger, B. A. Tannous, *Cells* **2019**, *8*, 1177.
[43] C. P. Lai, E. Y. Kim, C. E. Badr, R. Weissleder, T. R. Mempel, B. A. Tannous, X. O. Breakefield, *Nat. Commun.* **2015**, *6*, 7029.
[44] R. A. Haraszti, M. C. Didiot, E. Sapp, J. Leszyk, S. A. Shaffer, H. E. Rockwell, F. Gao, N. R. Narain, M. DiFiglia, M. A. Kiebish, N. Aronin, A. Khvorova, *J. Extracellular Vesicles* **2016**, *5*, 32570.
[45] C. C. Liang, A. Y. Park, J. L. Guan, *Nat. Protoc.* **2007**, *2*, 329.
[46] M. Vinci, C. Box, S. A. Eccles, *J. Vis. Exp.* **2015**, e52686.
[47] T. Wurdinger, C. Badr, L. Pike, R. de Kleine, R. Weissleder, X. O. Breakefield, B. A. Tannous, *Nat. Methods* **2008**, *5*, 171.
[48] C. E. Badr, J. M. Niers, L.-A. Tjon-Kon-Fat, D. P. Noske, T. Wurdinger, B. A. Tannous, *Mol. Imaging* **2009**, *8*, 278.
[49] C. C. Mandal, N. Ghosh-Choudhury, T. Yoneda, G. G. Choudhury, N. Ghosh-Choudhury, *J. Biol. Chem.* **2011**, *286*, 11314.
[50] B. Yamini, *Cells* **2018**, *7*, 125.
[51] V. Soubannier, S. Stifani, *Biomedicines* **2017**, *5*, 29.
[52] K. P. L. Bhat, K. L. Salazar, V. Balasubramaniyan, K. Wani, L. Heathcock, F. Hollingsworth, J. D. James, J. Gumin, K. L. Diefes, S. H. Kim, A. Turski, Y. Azodi, Y. Yang, T. Doucette, H. Colman, E. P. Sulman, F. F. Lang, G. Rao, S. Copray, B. D. Vaillant, K. D. Aldape, *Genes Dev.* **2011**, *25*, 2594.
[53] N. Syn, L. Wang, G. Sethi, J. P. Thiery, B. C. Goh, *Trends Pharmacol. Sci.* **2016**, *37*, 606.
[54] A. Segerman, M. Niklasson, C. Haglund, T. Bergström, M. Jarvius, Y. Xie, A. Westermark, D. Sönmez, A. Hermansson, M. Kastemar, Z. Naimaie-Ali, F. Nyberg, M. Berglund, M. Sundström, G. Hesselager, L. Uhrbom, M. Gustafsson, R. Larsson, M. Fryknäs, B. Segerman, B. Westermark, *Cell Rep.* **2016**, *17*, 2994.
[55] R. Lane, T. Simon, M. Vintu, B. Solkin, B. Koch, N. Stewart, G. Benstead-Hume, F. M. G. Pearl, G. Critchley, J. Stebbing, G. Giamas, *Commun. Biol.* **2019**, *2*, 315.
[56] D. Garnier, B. Meehan, T. Kislinger, P. Daniel, A. Sinha, B. Abdulkarim, I. Nakano, J. Rak, *Neuro-Oncology* **2018**, *20*, 236.
[57] Q. Zhang, R. X. Liu, K. W. Chan, J. Hu, J. Zhang, L. Wei, H. Tan, X. Yang, H. Liu, *J. Exp. Clin. Cancer Res.* **2019**, *38*, 320.
[58] M. S. Pavlyukov, H. Yu, S. Bastola, M. Minata, V. O. Shender, Y. Lee, S. Zhang, J. Wang, S. Komarova, J. Wang, S. Yamaguchi, H. A. Alsheikh, J. Shi, D. Chen, A. Mohyeldin, S. H. Kim, Y. J. Shin, K. Anufrieva, E. G. Evtushenko, N. V. Antipova, G. P. Arapidi, V. Govorun, N. B. Pestov, M. I. Shakhparonov, L. J. Lee, D. H. Nam, I. Nakano, *Cancer Cell* **2018**, *34*, 119.
[59] M. Fedele, L. Cerchia, S. Pegoraro, R. Sgarra, G. Manfioletti, *Int. J. Mol. Sci.* **2019**, *20*, 2746.
[60] J. V. Joseph, S. Conroy, T. Tomar, E. Eggens-Meijer, K. Bhat, S. Copray, A. M. E. Walenkamp, E. Boddeke, V. Balasubramanyian, M. Wagemakers, W. F. A. Den Dunnen, F. A. E. Kruyt, *Cell Death Dis.* **2014**, *5*, e1443.
[61] Y. Chen, R. Fang, C. Yue, G. Chang, P. Li, Q. Guo, J. Wang, A. Zhou, S. Zhang, G. N. Fuller, X. Shi, S. Huang, *Cancer Res.* **2020**, *80*, 1049.
[62] B. Ricci, T. O. Millner, N. Pomella, X. Zhang, L. Guglielmi, S. Badodi, D. Ceric, C. Gemma, E. Cognolato, Y. Zhang, S. Brandner, M. R. Barnes, S. Marino, *Oncogene* **2020**, *39*, 2523.
[63] Y. Zhang, A. Zeng, S. Liu, R. Li, X. Wang, W. Yan, H. Li, Y. You, *Oncol. Lett.* **2018**, *15*, 7625.
[64] W. Chen, K. K. Kong, X. K. Xu, C. Chen, H. Li, F. Y. Wang, X. F. Peng, Z. Zhang, P. Li, J. L. Li, F. C. Li, *Int. J. Oncol.* **2018**, *52*, 485.
[65] C. Li, H. Zheng, W. Hou, H. Bao, J. Xiong, W. Che, Y. Gu, H. Sun, P. Liang, *Cell Death Dis.* **2019**, *10*, 717.
[66] X. Du, Y. Tu, S. Liu, P. Zhao, Z. Bao, C. Li, J. Li, M. Pan, J. Ji, *J. Cell. Mol. Med.* **2020**, *24*, 1474.

